Loading of Halloysite Nanotubes with BSA, α-Lac and β-Lg: a Fourier Transform Infrared Spectroscopic and thermogravimetric study

Celia Duce[1], Valentina Della Porta[2], Emilia Bramanti[2]*, Beatrice Campanella[1,2], Alessio Spepi[1] and Maria Rosaria Tiné[1]

[1] University of Pisa, Department of Chemistry and Industrial Chemistry, Via G.Moruzzi 13, 56124 Pisa (Italy)

[2] National Research Council of Italy, C.N.R., Institute of Chemsitry of Organo Metallic Compounds-ICCOM- UOS Pisa, Area di Ricerca, Via G. Moruzzi 1, 56124 Pisa (Italy)

***Corresponding author**: Emilia Bramanti bramanti@pi.iccom.cnr.it

Revised version for *Nanotechnology* November 15th 2016

Abstract

Halloysite nanotubes (HNTs) are considered as ideal materials for biotechnological and medical applications. An important feature of halloysite is that it has a different surface chemistry on the inner and outer sides of the tubes. This property means that negatively-charged molecules can be selectively loaded inside the halloysite nanoscale its lumen. Loaded HNTs can be used for the controlled or sustained release of proteins, drugs, bioactive molecules and other agents.

We studied the interaction between HNTs and bovine serum albumin, α lactalbumin and β –lactoglobulin loaded into HTNs using Fourier Transform Infrared Spectroscopy and Thermogravimetry. These techniques enabled us to study the protein conformation and thermal stability, respectively, and to estimate the amount of protein loaded into the HNTs. TEM images confirmed the loading of proteins into HTNs.

Keywords: Halloysite nanotubes (HNTs); proteins; Fourier Transform Infrared Spectroscopy (FTIR); Thermogravimetry (TG)

1 Introduction

Materials based on nanoclays have attracted great interest because their properties and morphologies can be tuned. Halloysite nanotubes (HNTs) are newly emerging clays with unique features and innovative uses [15]. HNTs are considered to be “green”, i.e. supposedly not hazardous for the environment, cheap and abundantly available in natural deposits [36].

Due to the variety of crystallization conditions and geological occurrence, HNTs adopt various morphologies such as tubular, spheroidal and plate-like particles, of which the tubular structure is the most common and valuable [23]. Dried halloysite is a roll of 15–20 alumosilicate sheets with a packing periodicity of 0.72 nm with hollow lumens. Dimensions of the halloysite tubes vary depending on the deposit. Their outside diameter ranges between 50–100 nm, and the diameter of the internal lumen between 10–20 nm [36]. Due to their high length/diameter (L/D) ratio and superior high-temperature-resistant property, HNTs have been exploited to produce high-quality ceramics. Scientists and engineers have recently discovered and developed a large range of new applications for this material [23].

An important feature of Halloysite is its different surface chemistry at the inner and outer sides of the tubes; there is a silica layer on the outer surface of tube, while the alumina is on the inner (lumen) surface. Aluminium and silicon oxides have different ionization properties and surface charges. This is evident from the zeta-potentials of their colloids in water. Alumina has a positive charge of up to pH 8.5, while silica is negative above pH 1.5 [66]. Halloysite entraps molecules in various ways including adsorption to the external and internal walls of the tubes, intercalation within the interlayer space and, most importantly, by loading into lumen [36]. Halloysite can be selectively loaded with negatively-charged molecules inside the halloysite nanoscale lumen [36], from simple

organic and inorganic molecules to high molecular weight polymers, biologically active substances and biomolecules, including drugs, cosmetic additives, antiseptics, antibacterials, DNA, enzymes, and proteins [1, 2, 4, 33, 38, 56, 57, 62, 65, 66, 69].

HNTs are ideal biocompatible substrates for the controlled or sustained release of drugs or bioactive molecules in medical applications, additives for paints and sealants, lubricants, herbicides, pest repellents, household, food and personal products, cosmetics, and other agents [23]. An increasing number of studies have focused on the fabrication of polymer/HNT nanocomposites [23]. New materials based on HTNs have several unique advantages because they are low cost materials derived from natural resources and are environmentally friendly [67].

Studies on the thermal decomposition of natural Halloysite have shown that Halloysite loses the interlayer water and undergoes dehydroxilation below 600°C. However, surprisingly, the characteristic tubular morphology of halloysite is maintained up to 900 °C, even though the crystalline structure is destroyed leading to an amorphous structure [25, 30, 32, 46].

We studied the interaction of bovine serum albumin (BSA), alpha lactalbumin (α-Lac) and beta lactoglobulin (β-Lg) with the inner surface of HNTs using Fourier transform infrared spectroscopy (FTIR) and thermogravimetry (TG). FTIR spectroscopy is a valuable tool for investigating the conformational changes induced in protein secondary structures by their interaction with surfaces [7-9].

In this study we selected BSA, β-Lg and α-Lac as model for globular proteins because their structures and physicochemical properties are well characterized. Table 1 summarizes the physico-chemical properties of the three proteins.

Protein	MW (Da)	Isoelectric point (IEP)	Compactness	Dimensions (nm)	Net charge at pH 7	Zeta potential (mV)	Ref.
BSA	68,000	4.9	Soft	9.0×6.0×5.0	Negative	-14.6	[50]
β-LG	18,300	5.1	Hard	6.5×3.6×3.6	Negative	-19.5	[34]
α-LA	14,200	4.5	Soft	2.3×2.6×4.0	Negative	-7.3	[44]

Thanks to their biological abundance, these proteins are a model environment for potential interactions of engineered nanomaterials with biomolecules in the context of food and food processing. Moreover, these proteins are among the most studies in the framework of protein-nanoparticle interactions, thus constituting a reference for these kind of investigations. Serum albumin is the most abundant protein in mammalian plasma and BSA is the most studied serum protein due to its wide availability, low cost and high structural resemblance with human serum albumin. The most important property of BSA is its ability to bind reversibly to an incredible variety of ligands and it is the principal carrier of fatty acids that are otherwise insoluble in circulating plasma.

β-LG is also one of the most extensively studied proteins due to its high abundance in cow's milk. β-Lg is believed to function as transporters of some hydrophobic molecules such as retinol and long chain fatty acid molecules across the intestinal membrane.

We successfully applied the combined FTIR and TG approach to study the interaction of proteins with inorganic salts [24, 27, 43] and in the literature, these techniques have been applied to study protein-clay interactions [48]. Various spectroscopic techniques (NMR, fluorescence, and circular dichroism) are currently used to study protein structural conformations in solution. FTIR spectroscopy is best suited for comparing secondary structures for proteins in solution or adsorbed on a solid support.

2 Experimental

2.1 Materials and solutions

BSA (A-8531, 05470), α-Lac Type (L6010, Type III, calcium depleted) and β-Lg (L 3908, Types A and B) were purchased from Aldrich–Sigma Chemical Co and were used without further purification for all the experiments. Halloysite nanotubes were purchased from Sigma Aldrich (685445) and used without further purification.

Loading procedure. The following loading procedure was selected on the basis of the literature data [1-3, 33, 39, 57] in order to get the maximum amount of proteins loaded into HTNs. Solutions of BSA, α-Lac and β-Lg (2 mg/mL) were prepared by dissolving the lyophilized protein in ultrapure water. HNTs were added to the proteins solution in order to have HNTs/protein=1 weight ratio. Each protein suspension was magnetically stirred for 24 hours at room temperature (21 ± 1°C) and then divided into two aliquots. One aliquot was vortexed for 5 min and centrifuged at 4000 rpm for 10 minutes. Two protocols were then followed: in the first the residue was washed once with bidistilled water; in the second it was washed three times in order to completely remove the excess protein. The solid residue was left to dry under vacuum in the desiccator for two days (10^{-3} mbar). The dried residues were analysed by TG and ATR-FTIR. The aim was to highlight whether the protein had been adsorbed, or merely deposited on the surface of the nanotubes, and also to study the related TG signals.

The other aliquot was subjected to three vacuum cycles (1 hour vacuum + 1 hour magnetic stirring three times; membrane vacuum pump 0.0148 atm) then vortexed for 5 min, centrifuged at 4000 rpm for 10 minutes and washed three times (*loading*

procedure). The solution was left to dry under vacuum in the desiccator for two days. The dried residues were analysed by TG and ATR-FTIR.

A "blank" of the loading procedure (the same described above performed only on proteins without HTNs) allowed us to distinguish between the conformational changes due to the procedure with or without HTNs.

Ultrapure water was prepared with an Elga Purelab-UV system (Veolia Environment, Paris, France).

2.2 Equipment and measurements

2.2.1 Fourier transform infrared spectroscopy (FTIR)

FTIR spectra were recorded using a Perkin-Elmer Spectrum One FTIR spectrophotometer, equipped with a universal ATR accessory and a TGS detector. Measurements were performed in attenuated total reflectance (ATR) mode. In order to obtain a suitable S/N ratio, 128 interferograms were recorded averaged and Fourier-transformed to produce a spectrum with a nominal resolution of 4 cm^{-1}. An in-house LabVIEW program for peak fitting [11, 12] was employed to run the deconvolution of the Amide I band.

The LabVIEW program for peak fitting was based on a previous work [11, 12]. Prior to curve processing, a straight baseline passing through the ordinates at 1800 and 1480 cm^{-1} was subtracted, and spectra were normalized in the 1700 - 1600 cm^{-1} region. This approach was adopted in order to avoid artefacts in absorptions near the limits of the region examined (1700 - 1600 cm^{-1}). The second derivatives of the amide I band of the spectra examined (1700 - 1600 cm^{-1} region) were then analysed in order to determine the starting data (number and position of Gaussian components) required for the deconvolution procedure.

The choice of the amide I band for structural analysis is due to the very low contribution of the amino acid side chain absorptions present in this region [18], and to its higher intensity with respect to other amide modes. On the basis of the infrared assignment of amide components, assuming that the extinction coefficient is the same for all the secondary structures, the secondary structure composition can be obtained from the FTIR spectra. The percentage values of the various secondary structures were estimated by expressing the amplitude value of the bands assigned to each of these structures as a fraction of the total sum of the amplitudes of the Amide I components. The precision of the quantitative determination depends on the amounts of the structures in the protein. The coefficient of variation is < 10% for values of amide I component > 15%. While the general validity of the above assumption regarding the extinction coefficients remains to be tested, the good correlation found between the secondary structure results obtained by FTIR approaches and x-ray crystallography indicated that this is a reasonable assumption [11].

The spectroscopic estimation of the amount of protein adsorbed onto HTNs was performed on the basis of the Amide I optical density of the FTIR non-normalized spectrum recorded before and after rinsing to remove the excess BSA.

The deconvolution procedure was applied to the Amide I band of the FTIR spectra of proteins after rinsing in order to study the conformational changes of proteins adsorbed onto the clay.

2.2.2 Thermogravimetry (TG)

A TA Instruments Thermobalance model Q5000IR was used. Measurements were performed at a rate of 10°C/min, from 30 °C to 900°C under air flow (25 mL/min). The amount of samples in each TG measurement varied between 2 and 4 mg. Each

experiment was repeated three times. TG data were employed to estimate the yield of loading of BSA, α-Lac and β-Lg into HNTs using the following equation:

$$C_p = \frac{R_{HNTs} - R_S}{R_{HNTs} - R_B} * 100$$

where R_{HNTs} is the residual mass of HNTs, R_s is the residual mass of the HNTs/protein suspension, and R_B is the residual mass of protein blank, according to Odlyha et al. [42].

2.2.3. Transmission electron microscopy (TEM).

The size and morphology of the HTNs before and after loading with proteins were examined by transmission electron microscopy (TEM). The powders were suspended in 2 ml of isopropanol and a few drops of the suspensions were deposited onto copper grids. The solvent was then let to evaporate at room temperature. Images were acquired using a CM12 Philips transmission electron microscope equipped with a microanalysis Edax and LaB6 cathode.

2.2.4 Dynamic light scattering (DLS).

Dynamic Light Scattering (DLS) measurements of native BSA in water were performed using a Zetasizer Nano S (ZEN 1600) apparatus Malvern Instruments Ltd UK, equipped with a 4.0 mW laser (He-Ne, 632.8 nm). Scattering angle detection (173°) was measured by an avalanche photodiode. The BSA solutions were placed in a polystyrene cuvettes and held at 20 °C during analysis. Each sample was analized five times with 10-20 sub runs of ten seconds.

3 Results and discussion

3.1 Thermogravimetric study

Figures 1, 2 and 3 report the thermogravimetric curves (TG, panel A) and their corresponding derivatives (DTG, panel B) of pristine HNTs, lyophilized protein and protein loaded HNTs for BSA, α-Lac and β-Lg, respectively. Table 2 shows the experimental temperatures of and the percentage mass loss of the thermal degradation steps of pristine HNTs, lyophilized protein and protein loaded HNTs for BSA, α-Lac and β-Lg.

We chose as reference the thermogram of the lyophilized protein because we verified that in the absence of HTNs (blank) the thermal profiles of BSA, α-Lac and β-Lg did not change with protein treatments (magnetic stirring, vacuum cycles, drying). In addition, when the HTNs/protein mixtures were washed three times, the TG curves showed only the peaks due to HNTs thermal degradation (data not shown for brevity), indicating that the adsorbed proteins had been completely removed from the surface of the nanotubes. This indicates that the proteins interact only weakly (or do not interact at all) with the outer surface of the nanotubes. This result is important in order to confirm that any changes of the protein TG curves observed in the presence of HNTs are not due to the adsorption/loading procedures but are directly related to the interactions of the protein with the internal surfaces of the HNTs.

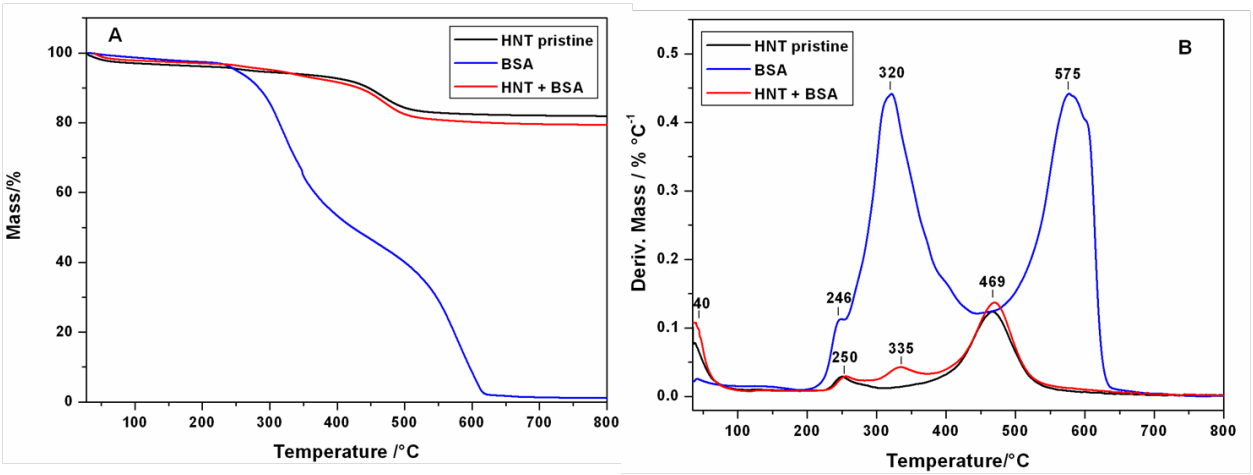

Figure 1. TG curves (panel A) and their corresponding DTG curves (panel B) of pristine HNTs (black line), lyophilized BSA (blue line), BSA loaded HNTs (red line) recorded under air flow at 10°C/min.

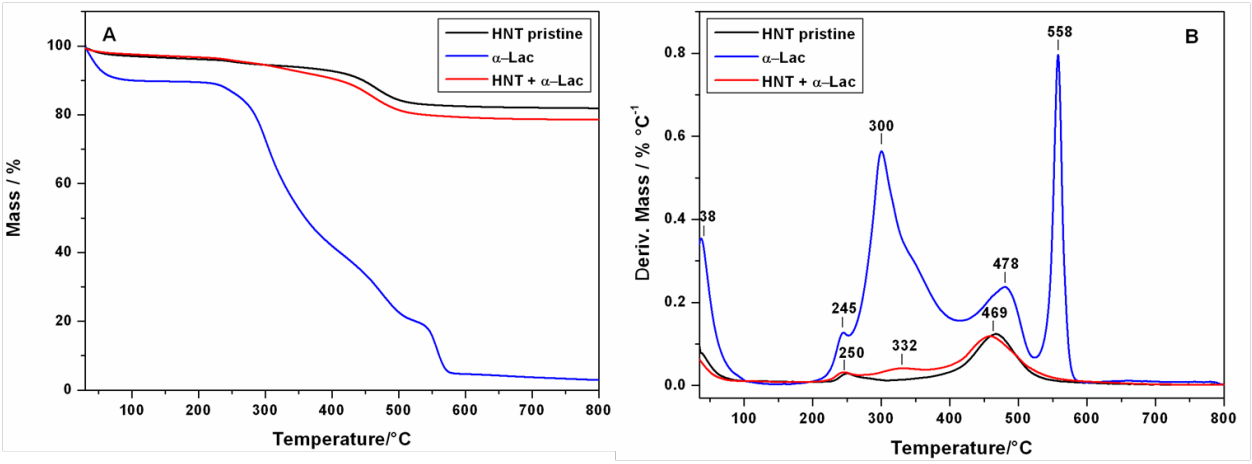

Figure 2. TG curves (panel A) and their corresponding TDG curves (panel B) of pristine HNTs (black line), lyophilized BSA (blue line), BSA loaded HNTs (red line) recorded under air flow at 10°C/min.

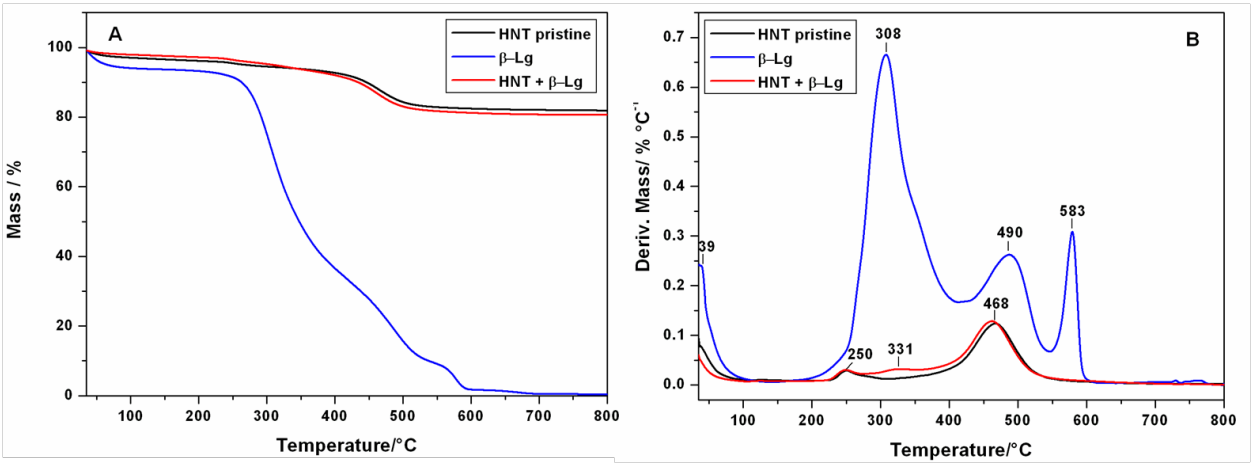

Figure 3. TG curves (panel A) and their corresponding DTG curves (panel B) of pristine HNTs (black line), lyophilized BSA (blue line), BSA loaded HNTs (red line) recorded under air flow at 10°C/min.

Table 2. Experimental temperatures of the thermal degradation steps of HNTs, pure proteins and proteins loaded into the HNTs.

Step number	***Temperature of the step (mass loss)***						
	HNTs	***BSA***	***BSA/ HNTs***	***α-Lac***	***α-Lac/ HNTs***	***β-Lg***	***β-Lg/ HNTs***
1	30 °C (3%)	40°C (1.4%)	40°C (2.2%)	38°C (7.0%)	36°C (2.9%)	39°C (6.2%)	35°C (2.1%)
2	250°C (2.5%)		250°C (2.1%)		250°C (1.9%)	-	250°C (2.0%)
3	-	320°C[a] (58.2%)	335°C (3.0%)	300°C[a] (52.8%)	332°C (3.4%)	308°C[a] (59.2%)	331°C (2.4%)

4	468°C (12.3%)	-	469°C (12.9%)	478°C (20.2%)	477°C (13.0%)	490°C (24.9%)	468°C (12.8%)
5	-	575° C [b] (38.2%)	-	558°C (15.8%)	-	583°C (7.9%)	-
Residue at 800°C	82.2%	2.2%	79.8%	4.2%	78.8%	1.8%	80.7%

[a] Total mass loss in the 200-400°C temperature range.

[a] Total mass loss in the 450-650°C temperature range.

HNTs undergo their three characteristic steps of mass loss due to the release of water physically adsorbed into the surface (below 50°C), the release of interlayer water molecules bound by hydrogen bonds (250°C), and the dehydroxylation process (470°C) [17, 28, 30].

Beside moisture evaporation (below 50°C), the decomposition of proteins under air flow shows a broad mass loss (more than 50%) with a maximum at 320°C for BSA, 300°C for α-Lac, and 308°C for β-Lg. There is also a shoulder at 245 (BSA and α-Lac), likely due to the polypeptide chain thermal decomposition of proteins [24, 26, 31]. In addition, BSA shows another broad mass loss (38%) in the range 450-650°C, while α-Lac and for β-Lg decompose into two steps at about 480 °C (20.2%) and 558 °C (15.8%) (α-Lac), and at 490°C (24.9%) and 580 °C (7.9%) (β-Lg).

Since it is known that BSA, (as well as ovalbumin), α-Lac and β-Lg may form dimers, oligomers and aggregated species [14, 60], the mass losses at 480 °C (α-Lac), and at 490°C (β-Lg) can be related to the decomposition of aggregated portions of proteins, while the sharp mass loss above 550°C (α-Lac and β-Lg) is likely related to the carbonizing and ashing of the hard residues of the proteins [26]. In the case of BSA, the

broad mass loss in the range 450-650°C includes both the decomposition of aggregates and the carbonizing and ashing of the hard residues of the proteins. The molecular weight of aggregates is obviously different and depends on the molecular weight and size of proteins: BSA MW 69.000 Da, 140Å x 40Å x 40Å [70], α-Lac MW 14.000 Da, 23Å x 26Å x 40Å [5] and β-Lg MW 18.000 Da, 3.8Å x 5Å x 5.7Å [55].

After the loading process, the TG curve of the HNTs/protein samples shows i) a 15-20°C shift toward higher temperatures of the protein mass loss at about 300°C, ii) a mass loss with a maximum at about 470°C due to both HNT and proteins decomposition, and iii) the disappearance of the protein mass loss at above 550 °C (Figure 1 and Table 2).

The 15-20°C shift toward higher temperatures of the protein mass loss at about 300°C can be ascribed to HNT/proteins interactions, but it seems too small to hypothesize a chemisorption of the protein on the inner HNT surface. It is likely due to the changes in the conformational structure of the proteins. There may also be small delay in the heat transmission due to the insulating properties of clays.

The conformational study described in the next section highlights that after the loading into the HTNs, the interaction of BSA and α-Lac with the inner surface of the HNTs leads to an increase in the beta structures with a consequent increase in their thermal stability. The interaction of β-Lg with the inner surface of the HNTs leads to an increase in the helix.

To explain the HNT/protein TG curve above 400°C, we can hypothesize that HTNs act as molecular sieves: only single protein molecules and small aggregates are allowed to be loaded into HTN lumina. The aggregates of α-Lac, β-Lg and BSA likely decompose in the same temperature range as the HNTs dehydroxylation. The higher molecular

weight aggregates of BSA are not present inside the HNTs and the ashing of the hard residues of the proteins does not occur for the proteins that are inside HNTs. In this case the formula reported in the Experimental underestimates the loading percentage of the HNTs. This formula, in fact, gives correct results if all the organic part of the sample is combusted in the experimental temperature range and the residue is only due to the inorganic material.

The loading yields obtained by using the values of residues at 800°C and the equation reported in the experimental section are of 3.2% for BSA, 4.1% for α-Lac and 1.1% for β-Lg; however these values may have been underestimated by up to 50%.

As an alternative approach, we calculated the weight percentage of protein loaded into HNTs by FTIR spectra following the equation:

$$\%\ \mathbf{protein\ adsorbed} = \left(\frac{\mathbf{ODr}}{\mathbf{ODnr}} * \boldsymbol{mg\ of\ protein / mg\ of\ total\ sample}\right) * \mathbf{100}$$

where ODr is the optical density of the Amide I band of the FTIR spectrum obtained on the dried film from protein/HTNs mixture after rinsing the protein excess, and ODnr is the optical density of the Amide I band of the FTIR spectrum obtained on the dried film from protein/HTNs mixture without rinsing the protein excess. We obtained a 12% loading for BSA, 8% for α-Lac, and 5% for β-Lg, in line with the best literature results [37, 63].

3.2 ATR-FTIR study

ATR-FTIR spectroscopy was used to study the protein conformation.

Figure 4 shows the representative FTIR spectra of lyophilized BSA, BSA treated with the loading procedure, and HNTs loaded with the protein and the FTIR spectrum of

loaded HNTs in the amide band region (1750-1450 cm^{-1}). The FTIR spectra of α-Lac and β-Lg are shown in the Supporting Informations.

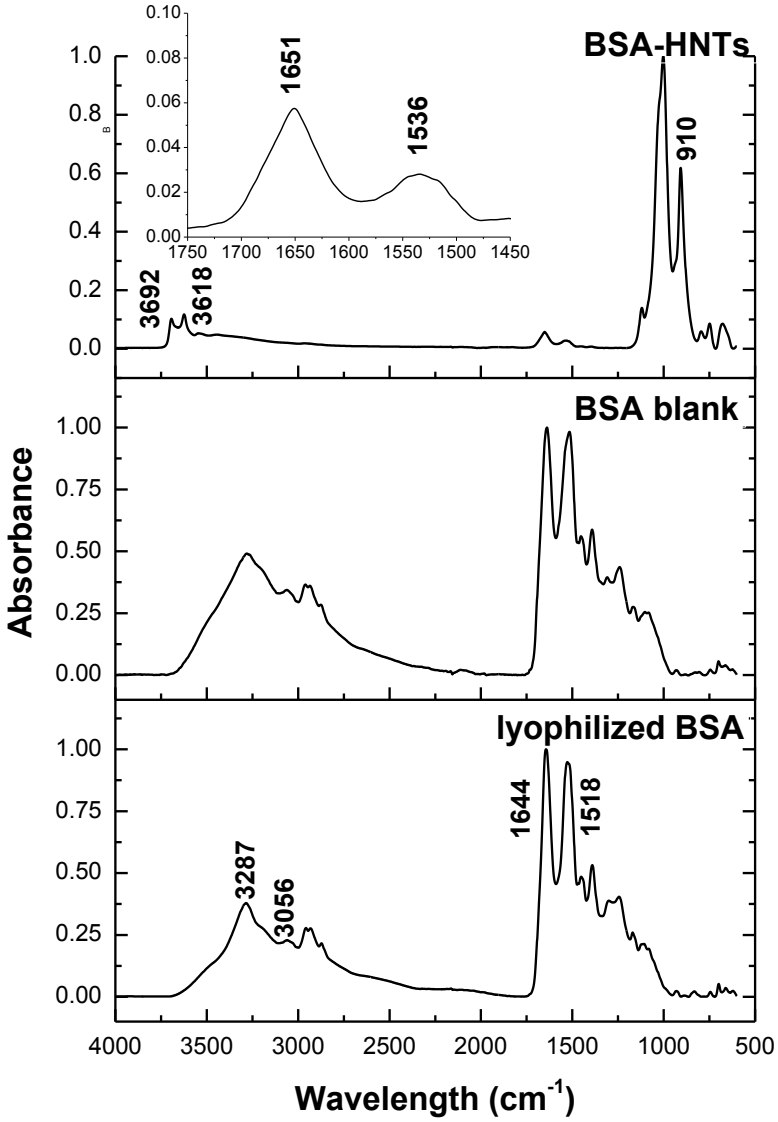

Figure 4. FTIR spectra of lyophilized BSA, BSA treated with the loading procedure, and HNTs loaded with BSA (inlet FTIR spectrum in the 1750–1450 cm^{-1} region).

The two characteristic bands of HNTs at 3696 and 3621 cm^{-1} are due to the stretching vibration of O–H in the inner-surface hydroxyl groups of Al–O–H. The absorption peak at 910 cm^{-1} is likely due to the deformation vibration of the above hydroxyl groups. The presence of the interlayer or adsorbed water is indicated by the stretching vibration at 3450 cm^{-1}. The spectrum of BSA has the characteristic bands of amide A (3282 cm^{-1}), amide B (3056 cm^{-1}), amide I, II, and III (respectively 1642, 1518 and 1234 cm^{-1}). No peaks of HNTs and Kao were present in the 1700–1250 cm^{-1} range.

The curve-fitting method described in the experimental section was applied to the deconvolution of the amide I band of the FTIR spectra in order to get detailed information on the secondary structure of BSA, α-Lac and β-Lg loaded into the HTNs. The results were compared to the secondary structures of lyophilized protein powders purchased from Sigma-Aldrich and of proteins prepared following the blank procedure, as described in the Experimental.

Figure 5 shows a representative plot of the curve fitting of the Amide I band of lyophilized BSA, BSA treated with the loading procedure (blank), and HNTs loaded with BSA.

Tables 3-5 show the quantitative results of the secondary structure analysis of BSA, α-Lac and β-Lg. Each invididual component of Amide I was assigned according to the literature [58, 68], namely *ca.* 1690 cm^{-1} (antiparallel β-sheets), *ca.* 1680 cm^{-1} (β turns), and *ca.* 1658 cm^{-1} (α-helix). The band in the 1626–1643 cm^{-1} region was assigned to β-sheets, and the band at 1641-1649 cm^{-1} was assigned to the random coil (wide peak width) or the solvated short helix (narrow peak width). The band at 1601–1617 cm^{-1} was assigned to inter-molecular β-sheets. Note that in our operating conditions the conformational changes observed were related to BSA loaded in HNTs. The excess BSA was, in fact, removed with the rinsing procedure (see Experimental).

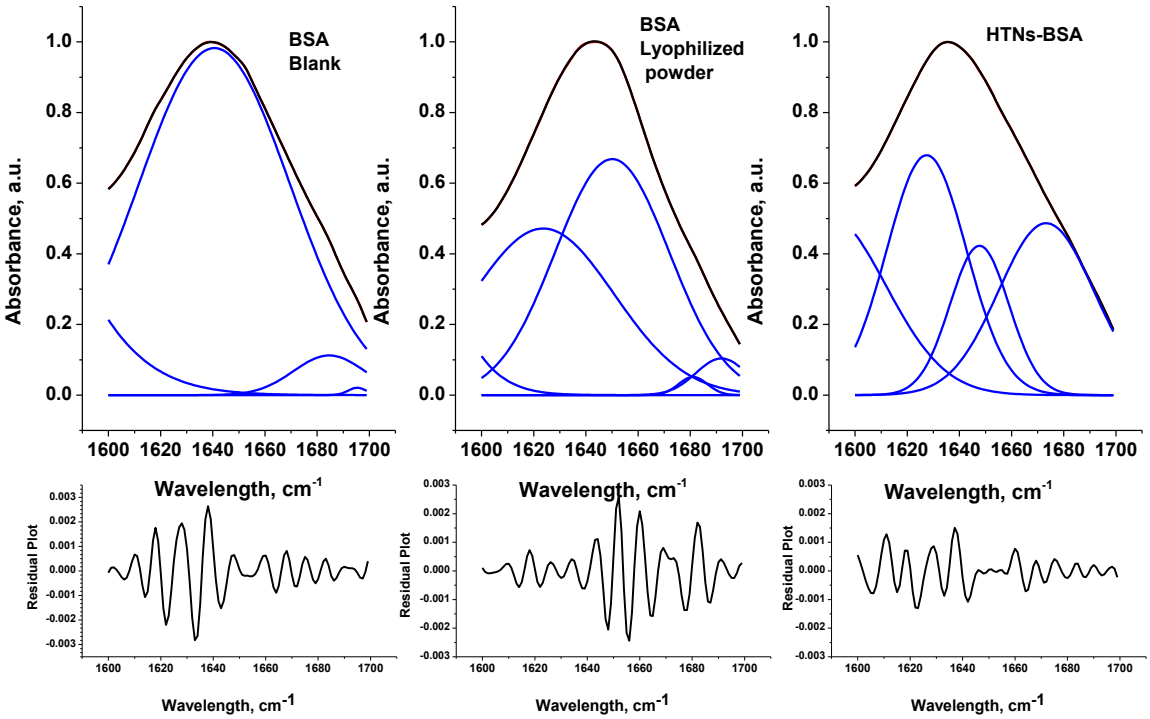

Figure 5. Representative plot of the curve fitting and the residual plots of the Amide I band of lyophilized BSA, BSA treated with the loading procedure (blank), and HNTs loaded with BSA. The residual plots have been calculated as difference spectrum measured (black line) and reconstructed one (red line).

Table 3. Results of the deconvolution procedure applied to the Amide I band of the FTIR spectra of BSA commercial lyophilized powder, BSA blank, and HNTs/BSA.

BSA powder ***Freq. (peak width)*** ***cm^{-1}*** ***%***	***BSA blank*** ***Freq. (peak width)*** ***cm^{-1}*** ***%***	***HNTs/BSA*** ***Freq. (peak width)*** ***cm^{-1}*** ***%***	***Assignment***
		-	Inter-molecular β sheets
1623 (64) 36%		1635 (49) 40%	β sheets
	1641(68) 87%		Random coil
1651 (51) 51%		1653 (28) 29%	α Helix
1681 (13) 5%	1684 (32) 11%	1680 (43) 31%	β Turns
1691 (23) 8%	1695 (8) 2%		β sheets ap

Table 4. Results of the deconvolution procedure applied to the Amide I band of the FTIR spectra of α-Lac powder, α-Lac blank, and HNTs/ α-Lac.

α-Lac powder ***Freq. (peak width)*** ***cm^{-1}*** ***%***	***α-Lac blank*** ***Freq. (peak width)*** ***cm^{-1}*** ***%***	***HNTs/α-Lac*** ***Freq. (peak width)*** ***cm^{-1}*** ***%***	***Assignment***
	1615 (17) 3%	1603 (18) 7%	Inter-molecular β sheets
	1634 (37) 40%	1623 (33) 21%	β sheets
1645 (52) 73%			Random coil
	1657 (28) 22%	1652 (36) 50%	α Helix
1674 (24) 13%	1684 (23) 30%	1675 (19) 6%	β Turns
1692 (24) 14%	1699 (14) 5%	1687 (34) 16%	β sheets ap

Table 5. Results of the deconvolution procedure applied to the Amide I band of the FTIR spectra of β-Lg powder, β-Lg blank, and HNTs/β-Lg.

β-Lg powder ***Freq. (peak width)*** ***cm^{-1}*** ***%***	***β-Lg blank*** ***Freq. (peak width)*** ***cm^{-1}*** ***%***	***HNTs/β-Lg*** ***Freq. (peak width)*** ***cm^{-1}*** ***%***	***Assignment***
1620 (35) 37%		1609 (11) 3%	Inter-molecular β sheets
1633 (20) 11%	1627 (36) 43%	1630 (47) 31%	β sheets
1646 (13) 4%	1648 (27) 28%		Solvated short α-helix
1654 (44) 38%		1656 (69) 64%	α Helix
1686 (30) 10%	1673 (43) 29%		β Turns
		1694 (18) 2%	β sheets ap

Figure 6 summarizes the percentage of the protein secondary structure components (β-structures, helix and random coil) of BSA, α-Lac and β-Lg lyophilized powder, as well as protein blanks and proteins loaded into HTNs. The contribution of β structures is calculated as the sum of antiparallel β-sheets, β turns, intra molecular and intermolecular β sheets. The helix percentage is calculated as the sum of the α-helix and the solvated short helix.

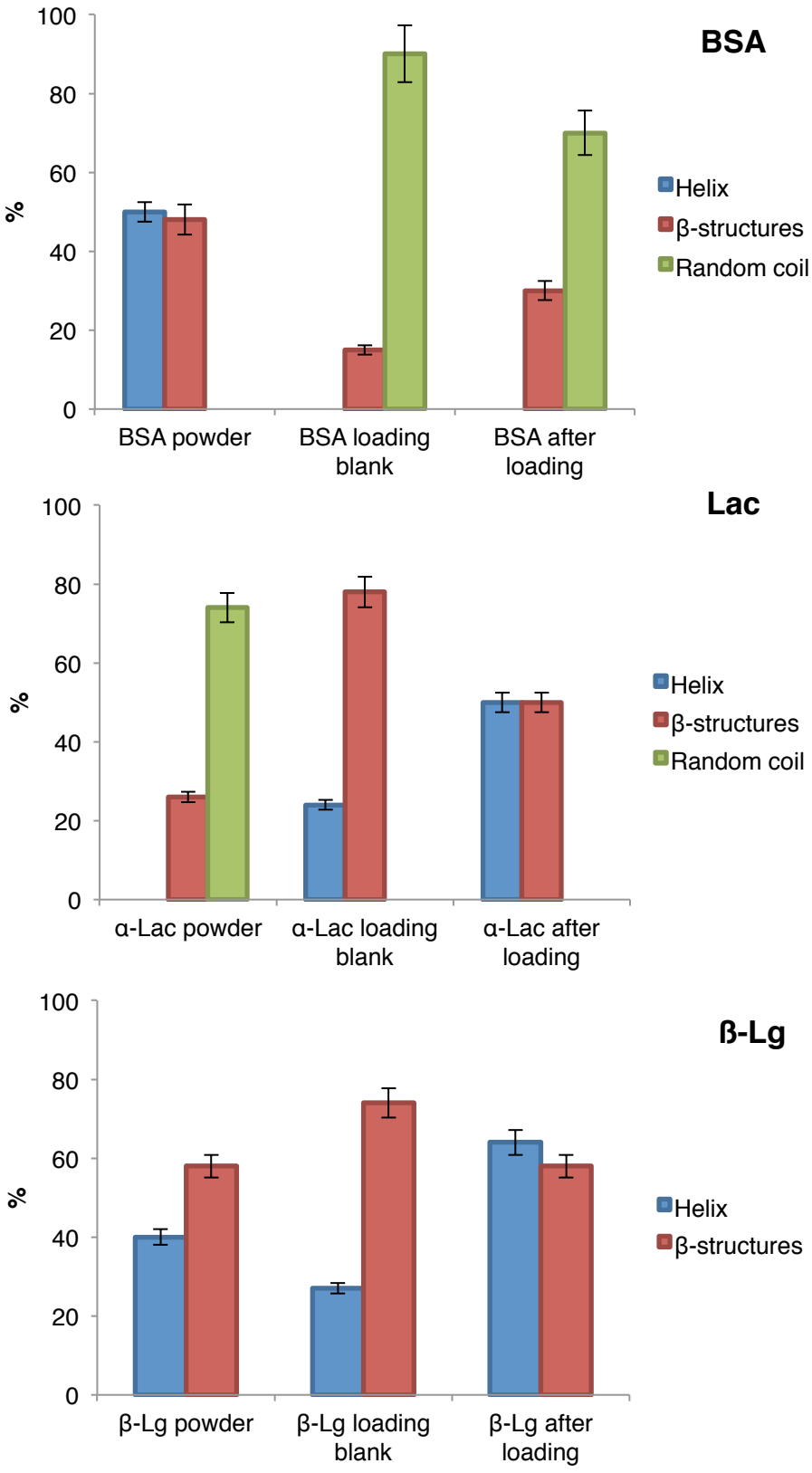

Figure 6. Secondary structure percentages of protein powder, protein after the loading blank procedure and HNTs/protein samples.

The FTIR data of BSA lyophilized powder (Figure 6A) shows that BSA is in its native state, since the secondary structure percentages are in agreement with those reported in the literature [11, 13, 16, 29, 49, 59]. The dissolution of 2 mg/mL BSA in bidistilled water and the treatment of the solution with vacuum cycles, magnetic stirrings, centrifugation and drying under vacuum (blank as described in the Experimental) led to the disruption of ordered structures and the almost complete unfolding of BSA. The random coil structure reached 87%. The loading of BSA into the HNTs lumen led, instead, to a refolding of BSA in a non-native conformation but characterized by ordered structures: 71% β structures and 29% α-helix. Considering that the isoelectric point (pI) of BSA is 4.7 [45], in water BSA has a negative net charge, and the electrostatic interactions are the driving forces between the negative BSA molecules and the positive surface of the inner layer of HNTs. This interaction induces a more compact, ordered structure. This result is in agreement with a previous study that showed that the surface curvature stabilizes the secondary structure of albumin [52].

The secondary structure of α-Lac lyophilized powder (Figure 6B) had a high percentage of random coil (73%) because it is Ca^{++} depleted [21, 35]. The blank procedure gave a conversion of random coil into α-helix (22%) and β-structures (78%), likely due to the relatively high concentration of α-Lac solution (2 mg/mL, i.e. about 110 μM). The basic and acid side chains of protein amino acids likely act as a buffer [19].

The loading of α-Lac into HNTs lumen led to an increase in α-helix structures (50%) and a decrease in the β-structures (50%). Again, the negative charge of protein (pI=4.2) favours its interaction with the positive inner surface of HNTs, inducing a rearrangement of α-Lac secondary structure into a native-like state. Although α-Lac has been reported

to contain 31% α-helix [5] and about 21% 3_{10}-helix [51, 61, 64], which are easily identifiable in FTIR spectra, the secondary structure of the loaded α-Lac showed only the α-helix structure.

The deconvolution procedure of β-Lg lyophilized powder (Figure 6C) confirmed that β-Lg is native [10, 22, 47, 54]. The dissolution of 2 mg/mL β-Lg in bidistilled water treated with the blank procedure caused significant conformational changes. In particular, we observed the disappearance of intermolecular β-sheets with their conversion in intra-molecular β-sheets, their increase, and the decrease in the α-helix.

β-Lg loaded into HNTs showed the loss of β components and a notable increase in the α-helix (64%). In our operating conditions, β-Lg is closer than BSA and α-Lac to its pI (pI=5.2). Again, although less advantageous, the electrostatic interactions between negative charges of β-Lg and the positively charged inner surface of HNTs are possibly responsible for these conformational changes.

These results are in agreement with studies performed in the past few years on a variety of nanoparticles of various dimensions, composition and surface characteristics that have been investigated to understand the mechanism of interaction with proteins [40]. Electrostatic and hydrophobic interactions, alone or in combination are considered to be the basis of the interaction between nanomaterials and protein, and this depends on the nature and source of nanoparticles and the proteins investigated [39, 41].

3. TEM study of HTNs loaded with BSA

A representative TEM study of HTNs loaded with BSA was performed to support TG and FTIR data.

Figure 7 shows TEM pictures of HNTs (A and B) and HNT loaded with BSA (C and D). The nanotubes' lumen and external/internal diameters, as well as the particle size are indicated by the red lines.

The nanotubes appeared to form large clusters in the micrometer range. Despite the formation of such agglomerates, the tubular and elongated structure of each nanoparticle can still be clearly identified in both loaded and not loaded HNTs [20].

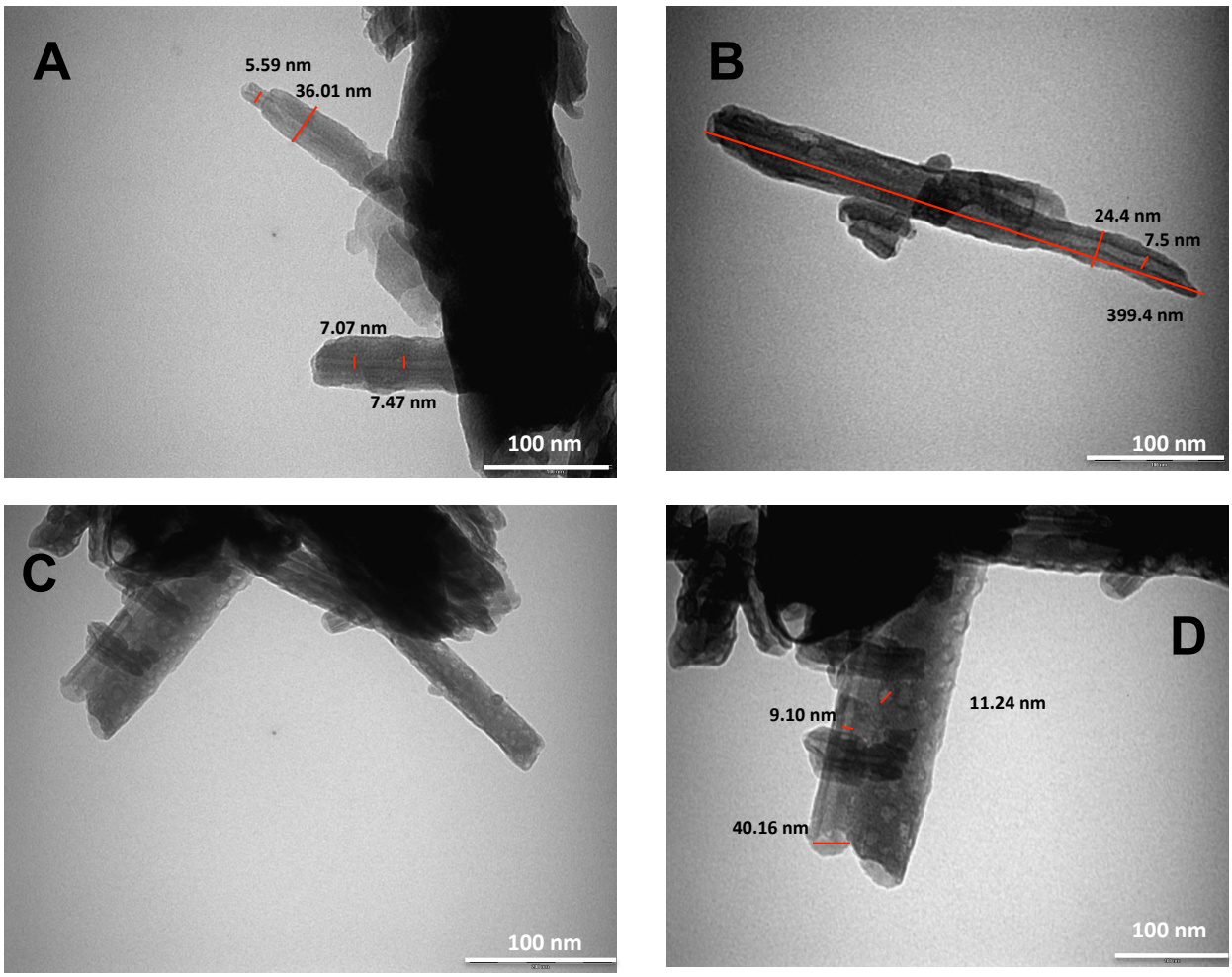

Figure 7. TEM pictures of HNTs (A and B) and HNT loaded with BSA (C and D). The nanotubes' lumen and external/internal diameters, as well as the organic particle size (D) are indicated by the red lines.

The TEM pictures of the HNTs confirmed the hollow nanostructure of the halloysite clay. Not loaded HTNs had a external and inner diameter of 30,2 ± 8.2 nm and 6.9 ± 1, respectively, and a strongly elongated structure, which appeared to have a high ratio between diameter and length, usually higher than 5-10. HTNs loaded with BSA had a bigger external and inner diameter of the not loaded HTNs was When loaded both the external and the diameters were higher: 40.2 ± 2 nm and 9 ± 1.5 nm, respectively. This result suggested that the protein molecules were present in the lumen and between the layers.

The ligth gray spots in Figure 7 C and D are organic material, likely BSA, as reported also by de Kruif et al. [20]. Their diameter was 11 ± 1 nm, about 3 times higher than the size of native BSA. DLS data of 0.1-0.5 mg/mL native BSA in bidistilled ultrapure water showed, indeed, a single peak distribution (Figure S3 of the Supporting Information) with particles ranging between 3-4 nm, in agreement with the literature data (3.2-3.9 nm as reported in [6, 53]). This result is compatible with the structural changes found by the FTIR study as well as with the formation of small aggregates (likely trimers).

Figure 7 C and D also show that the external surface of HTNs after protein loading is rougher and less defined. This may suggest the BSA adsorption on the external HNT surface in addition to the penetration into the HTNs.

4. Conclusions

We exploited TG and FTIR spectroscopy to study the thermal stability and conformational changes of BSA, β-Lg and α-Lac after they had been loaded into HTNs.

We observed that the thermal degradation of proteins loaded into HNTs lumen occurred at temperatures higher than those of free proteins. This increase in the thermal stability

may be due to the changes in the secondary structure driven by the interaction with HNTs.

Our FTIR data showed that the dissolution of proteins in water itself and the treatment of the solution with vacuum cycles, magnetic stirrings, centrifugation and drying under vacuum led to several conformational changes in the proteins, which are different from the changes in the protein secondary structure observed after they have been loaded into HNTs. In all cases, we found that the proteins loaded into HNTs lumen had ordered structures (β structures and helices). The electrostatic interactions between the negative charge of proteins and the positive inner surface of HNTs are likely responsible for the protein adsorption and, thus, for the conformational changes in the proteins. TEM data confirmed the loading of proteins into HTNs.

All these findings indicate that possible applications of HNTs as protein carriers in biotechnology and nanomedicine cannot ignore the fact that nanostructures may cause deep conformational changes in the proteins and this may dramatically alter the properties of these proteins.

ACKNOWLEDGEMENTS

This work was supported by the projects FIRB 2012 (No. RBFR12ETL5), funded by the Italian Ministry of University and Research, and PRA_2016_46 funded by the University of Pisa.

Bibliography

[1] Abdullayev E and Lvov Y 2010 Clay nanotubes for corrosion inhibitor encapsulation: release control with end stoppers *Journal of Materials Chemistry* **20** 6681-7

[2] Abdullayev E and Lvov Y 2011 Halloysite Clay Nanotubes for Controlled Release of Protective Agents *Journal of Nanoscience and Nanotechnology* **11** 10007-26

[3] Abdullayev E, Price R, Shchukin D and Lvov Y 2009 Halloysite Tubes as Nanocontainers for Anticorrosion Coating with Benzotriazole *ACS Applied Materials & Interfaces* **1** 1437-43

[4] Abdullayev E, Sakakibara K, Okamoto K, Wei W, Ariga K and Lvov Y 2011 Natural Tubule Clay Template Synthesis of Silver Nanorods for Antibacterial Composite Coating *ACS Applied Materials & Interfaces* **3** 4040-6

[5] Acharya K R, Stuart D I, Walker N P C, Lewis M and Phillips D C 1989 Refined structure of baboon α-lactalbumin at 1.7 Å resolution: Comparison with C-type lysozyme *Journal of Molecular Biology* **208** 99-127

[6] Alexander J. S. Chapman D M G 2011 Measurements of hydrodynamic radius for a standard protein over a wide concentartion range.

[7] Barth A 2007 Infrared spectroscopy of proteins *Biochimica et Biophysica Acta (BBA) - Bioenergetics* **1767** 1073-101

[8] Barth A and Haris P I 2009 *Biological and Biomedical Infrared Spectroscopy* vol vol. 2 (Amsterdam, Netherlands: IOS Press)

[9] Barth A and Zscherp C 2002 What vibrations tell about proteins *Quarterly Reviews of Biophysics* **35** 369--430

[10] Böhm G, Muhr R and Jaenicke R 1992 Quantitative analysis of protein far UV circular dichroism spectra by neural networks *Protein Engineering* **5** 191-5

[11] Bramanti E and Benedetti E 1996 Determination of the secondary structure of isomeric forms of human serum albumin by a particular frequency deconvolution procedure applied to Fourier transform IR analysis *Biopolymers* **38** 639-53

[12] Bramanti E, Bramanti M, Stiavetti P and Benedetti E 1994 A FREQUENCY DECONVOLUTION PROCEDURE USING A CONJUGATE-GRADIENT MINIMIZATION METHOD WITH SUITABLE CONSTRAINTS *Journal of Chemometrics* **8** 409-21

[13] Cai S and Singh B R 1999 Identification of β-turn and random coil amide III infrared bands for secondary structure estimation of proteins *Biophysical Chemistry* **80** 7-20

[14] Campanella B, Onor M, D'Ulivo A, Giannarelli S and Bramanti E 2014 Impact of protein concentration on the determination of thiolic groups of ovalbumin: a size exclusion chromatography-chemical vapor generation-atomic fluorescence spectrometry study via mercury labeling *Analytical chemistry* **86** 2251-6

[15] Cavallaro G, Donato D I, Lazzara G and Milioto S 2011 Films of Halloysite Nanotubes Sandwiched between Two Layers of Biopolymer: From the Morphology to the Dielectric, Thermal, Transparency, and Wettability Properties *The Journal of Physical Chemistry C* **115** 20491-8

[16] Chen Y H, Yang, J. T., and Chau, K. H. (1974). Biochemistry 13, 3350-3359.

[17] Cheng H, Yang J, Liu Q, He J and Frost R L 2010 Thermogravimetric analysis–mass spectrometry (TG–MS) of selected Chinese kaolinites *Thermochimica Acta* **507–508** 106-14

[18] Chirgadze Y N, Fedorov O V and N.P. T 1975 Estimation of amino acid residue side-chain absorption in the infrared spectra of protein solutions in heavy water *Biopolymers* **14** 679-94
[19] Christensen H N 1966 PROTEINS AS BUFFERS *Annals of the New York Academy of Sciences* **133** 34-40
[20] de Kruif J K, Ledergerber G, Garofalo C, Fasler-Kan E and Kuentz M 2016 On prilled Nanotubes-in-Microgel Oral Systems for protein delivery *European Journal of Pharmaceutics and Biopharmaceutics* **101** 90-102
[21] Demarest S J, Boice J A, Fairman R and Raleigh D P 1999 Defining the core structure of the α-lactalbumin molten globule state1 *Journal of Molecular Biology* **294** 213-21
[22] Dong A, Matsuura J, Allison S D, Chrisman E, Manning M C and Carpenter J F 1996 Infrared and Circular Dichroism Spectroscopic Characterization of Structural Differences between β-Lactoglobulin A and B *Biochemistry* **35** 1450-7
[23] Du M, Guo B and Jia D 2010 Newly emerging applications of halloysite nanotubes: a review *Polymer International* **59** 574-82
[24] Duce C, Bramanti E, Ghezzi L, Bernazzani L, Bonaduce I, Colombini M P, Spepi A, Biagi S and Tine M R 2013 Interactions between inorganic pigments and proteinaceous binders in reference paint reconstructions *Dalton Transactions* **42** 5975-84
[25] Duce C, Ciprioti S V, Ghezzi L, Ierardi V and Tine M R 2015 Thermal behavior study of pristine and modified halloysite nanotubes A modern kinetic study *Journal of Thermal Analysis and Calorimetry* **121** 1011-9
[26] Duce C, Ghezzi L, Onor M, Bonaduce I, Colombini M, Tine' M and Bramanti E 2012 Physico-chemical characterization of protein–pigment interactions in tempera paint reconstructions: casein/cinnabar and albumin/cinnabar *Anal Bioanal Chem* **402** 2183-93
[27] Duce C, Ghezzi L, Onor M, Bonaduce I, Colombini M P, Tine M R and Bramanti E 2012 Physico-chemical characterization of protein-pigment interactions in tempera paint reconstructions: casein/cinnabar and albumin/cinnabar *Anal Bioanal Chem* **402** 2183-93
[28] Duce C V C S, Ghezzi L, Tinè MR, Thermal behavior study of pristine and modified halloysite nanotubes. A modern kinetic study. J Therm Anal Calorim. 2015. doi:10. 1007/ s10973-015-4741-7. 2015
[29] Foster J F 1977 *Albumin: Structure, Function and Uses,* ed V M R O A Rothschild: Pergamon) pp 53-84
[30] García F J, García Rodríguez S, Kalytta A and Reller A 2009 Study of Natural Halloysite from the Dragon Mine, Utah (USA) *Zeitschrift für anorganische und allgemeine Chemie* **635** 790-5
[31] Ghezzi L, Duce C, Bernazzani L, Bramanti E, Colombini M P, Tine M R and Bonaduce I 2015 Interactions between inorganic pigments and rabbit skin glue in reference paint reconstructions *Journal of Thermal Analysis and Calorimetry* **122** 315-22
[32] Johnson S L, Guggenheim S and Koster Van Groos A F 1990 Thermal stability of halloysite by high-pressure differential thermal analysis *Clays & Clay Minerals* **38** 477-84
[33] Joshi A, Abdullayev E, Vasiliev A, Volkova O and Lvov Y 2013 Interfacial Modification of Clay Nanotubes for the Sustained Release of Corrosion Inhibitors *Langmuir* **29** 7439-48

[34] Kawasaki K, Kambara M, Matsumura H and Norde W 2003 A comparison of the adsorption of saliva proteins and some typical proteins onto the surface of hydroxyapatite *Colloids and Surfaces B: Biointerfaces* **32** 321-34
[35] Kuwajima K 1989 The molten globule state as a clue for understanding the folding and cooperativity of globular-protein structure *Proteins: Structure, Function, and Bioinformatics* **6** 87-103
[36] Lvov Y and Abdullayev E 2013 Functional polymer–clay nanotube composites with sustained release of chemical agents *Progress in Polymer Science* **38** 1690-719
[37] Lvov Y, Aerov A and Fakhrullin R 2014 Clay nanotube encapsulation for functional biocomposites *Advances in Colloid and Interface Science* **207** 189-98
[38] Lvov Y M, Shchukin D G, Möhwald H and Price R R 2008 Halloysite Clay Nanotubes for Controlled Release of Protective Agents *ACS Nano* **2** 814-20
[39] Lynch I and Dawson K A 2008 Protein-nanoparticle interactions *Nano Today* **3** 40-7
[40] Mandal S, Hossain M, Devi P S, Kumar G S and Chaudhuri K 2013 Interaction of carbon nanoparticles to serum albumin: elucidation of the extent of perturbation of serum albumin conformations and thermodynamical parameters *Journal of hazardous materials* **248-249** 238-45
[41] Mu Q X, Liu W, Xing Y H, Zhou H Y, Li Z W, Zhang Y, Ji L H, Wang F, Si Z K, Zhang B and Yan B 2008 Protein binding by functionalized multiwalled carbon nanotubes is governed by the surface chemistry of both parties and the nanotube diameter *J. Phys. Chem. C* **112** 3300-7
[42] Odlyha M, Cohen N S, Foster G M and West R H 2000 Dosimetry of paintings: determination of the degree of chemical change in museum exposed test paintings (azurite tempera) by thermal and spectroscopic analysis *Thermochimica Acta* **365** 53-63
[43] Pellegrini D, Duce C, Bonaduce I, Biagi S, Ghezzi L, Colombini M P, Tine M R and Bramanti E 2016 Fourier transform infrared spectroscopic study of rabbit glue/inorganic pigments mixtures in fresh and aged reference paint reconstructions *Microchemical Journal* **124** 31-5
[44] Permyakov E A and Berliner L J 2000 α-Lactalbumin: structure and function *FEBS Letters* **473** 269-74
[45] Pierce K M, Bramanti E, Onor M, Spiniello R, Kangas A, Skogerboe K J and Synovec R E 2010 Analysis of commercial beverage products by size exclusion chromatography coupled with UV-vis absorbance detection and dynamic surface tension detection *Talanta* **80** 1445-51
[46] Presti D, Pedone A, Mancini G, Duce C, Tine M R and Barone V 2016 Insights into structural and dynamical features of water at halloysite interfaces probed by DFT and classical molecular dynamics simulations *Physical Chemistry Chemical Physics* **18** 2164-74
[47] Qi P X, Wickham E D and Garcia R A 2014 Structural and Thermal Stability of beta-Lactoglobulin as a Result of Interacting with Sugar Beet Pectin *J. Agric. Food Chem.* **62** 7567-76
[48] Rangel-Porras G, Rangel-Rivera P, Pfeiffer-Perea H and Gonzalez-Muñoz P 2015 Changes in the characteristics of acid-treated clay after the inclusion of proteins *Surf. Interface Anal.* **47** 7

[49] Reed R G, Feldhoff R C, Clute O L and Peters Jr T 1975 Fragments of bovine serum albumin produced by limited proteolysis. Conformation and ligand binding *Biochemistry* **14** 4578-83
[50] Rezwan K, Studart A R, Vörös J and Gauckler L J 2005 Change of ζ Potential of Biocompatible Colloidal Oxide Particles upon Adsorption of Bovine Serum Albumin and Lysozyme *The Journal of Physical Chemistry B* **109** 14469-74
[51] Richardson J S 1981 *Advances in Protein Chemistry,* ed J T E C.B. Anfinsen and M R Frederic: Academic Press) pp 167-339
[52] Roach P, Farrar D and Perry C C 2006 Surface tailoring for controlled protein adsorption: Effect of topography at the nanometer scale and chemistry *J. Am. Chem. Soc.* **128** 3939-45
[53] Rob Meijers E 2012 Sample preparation and characterization around SAXS.
[54] Sardar S, Pal S, Maity S, Chakraborty J and Halder U C 2014 Amyloid fibril formation by β-lactoglobulin is inhibited by gold nanoparticles *International Journal of Biological Macromolecules* **69** 137-45
[55] Sawyer L, Kontopidis G and Wu S-Y 1999 β-Lactoglobulin – a three-dimensional perspective *International Journal of Food Science & Technology* **34** 409-18
[56] Shamsi M H and Geckeler K E 2008 The first biopolymer-wrapped non-carbon nanotubes *Nanotechnology* **19**
[57] Shchukin D G, Sukhorukov G B, Price R R and Lvov Y M 2005 Halloysite Nanotubes as Biomimetic Nanoreactors *Small* **1** 510-3
[58] Shi X, Li D, Xie J, Wang S, Wu Z and Chen H 2012 Spectroscopic investigation of the interactions between gold nanoparticles and bovine serum albumin *Chin. Sci. Bull.* **57** 1109-15
[59] Sjoholm I and Ljungstedt I 1973 Studies on the tryptophan and drug binding properties of human serum albumin fragments by affinity chromatography and circular dichroism measurements *Journal of Biological Chemistry* **248** 8434-41
[60] Staggemeier B A, Bramanti E, Allegrini C, Skogerboe K J and Synovec R E 2005 High-throughput screening of protein surface activity via flow injection analysis-pH gradient-dynamic surface tension detection *Analytical chemistry* **77** 250-8
[61] Sudha T S, Vijayakumar E K S and Balaram P 1983 Circular dichroism studies of helical oligopeptides: Can 310 and α-helical conformations be chiroptically distinguished? *International Journal of Peptide and Protein Research* **22** 464-8
[62] Suh Y J, Kil D S, Chung K S, Abdullayev E, Lvov Y M and Mongayt D 2011 Natural Nanocontainer for the Controlled Delivery of Glycerol as a Moisturizing Agent *Journal of Nanoscience and Nanotechnology* **11** 661-5
[63] Tully J, Yendluri R and Lvov Y 2016 Halloysite Clay Nanotubes for Enzyme Immobilization *Biomacromolecules* **17** 615-21
[64] Urbanova M, Dukor R K, Pancoska P, Gupta V P and Keiderling T A 1991 Comparison of .alpha.-lactalbumin and lysozyme using vibrational circular dichroism. Evidence for a difference in crystal and solution structures *Biochemistry* **30** 10479-85
[65] Veerabadran N G, Mongayt D, Torchilin V, Price R R and Lvov Y M 2009 Organized Shells on Clay Nanotubes for Controlled Release of Macromolecules *Macromolecular Rapid Communications* **30** 99-103
[66] Veerabadran N G, Price R R and Lvov Y M 2007 Clay nanotubes for encapsulation and sustained release of drugs *Nano* **2** 115-20

[67] Vergaro V, Abdullayev E, Lvov Y M, Zeitoun A, Cingolani R, Rinaldi R and Leporatti S 2010 Halloysite clay nanotubes: Characterization, biocompatibility and use as drug carriers(vol 3) p 395-6
[68] Wang H D, Niu C H, Yang Q Q and Badea I 2011 Study on protein conformation and adsorption behaviors in nanodiamond particle-protein complexes *Nanotechnology* **22**
[69] Wang S, Zhao J, Hu F, Li X, An X, Zhou S, Chen Y and Huang M 2016 Phase-Changeable and Bubble-Releasing Implants for Highly Efficient HIFU-responsive Tumor Surgery and Chemotherapy *Journal of Materials Chemistry B*
[70] Wright A K and Thompson M R 1975 Hydrodynamic structure of bovine serum albumin determined by transient electric birefringence *Biophysical Journal* **15**